AIAA 82-4234

Choking Analysis for a cw HF or DF Chemical Laser

George Emanuel*
University of Oklahoma, Norman, Oklahoma

This study investigates choking in the optical cavity of a cw HF or DF chemically-pumped laser. Choking can occur because of the large heat release when the flow in the cavity is constrained by plume shrouds. An analysis procedure is described that starts in the oxidizer and fuel plenums, follows both gases through the nozzles where the flow is viscous, and into a constant area laser cavity where mixing and heat addition occur. A parametric investigation is performed that centers around a He diluent case and a N_2 diluent case. The parameters that are varied include plenum conditions, composition, nozzle geometry, etc. The most important results are 1) a He diluent flow is more likely to choke than one with N_2, 2) the oxidizer stagnation temperature and oxidizer diluent ratio are dominant choking parameters, 3) shifting diluent from the oxidizer to the fuel flow can lead to choking, 4) nozzle geometry has a minor effect on choking, and 5) Reynolds number scaling for choking is demonstrated.

Nomenclature

a = speed of sound
A = cross-sectional area
C_i = viscosity coefficient
H = total enthalpy
ΔH = heat of reaction
j_1 = 0 for He, 1 for N_2 primary diluent
j_2 = 0 for H_2, 1 for D_2 cavity fuel
J = impulse
$\dot{m}$ = mass flow rate
M = Mach number
$\dot{N}$ = molar flow rate
p = pressure
P = laser outcoupled power
R = universal gas constant
R = radius at nozzle exit
Re = Reynolds number
R_L = fuel/oxidizer ratio
s = arc length
T = temperature
u = velocity
W = molecular weight
X = mole fraction
y = transverse coordinate
Z_m = dimensionless mixing parameter
Z_r = dimensionless heat addition parameter
α = F/F_2 mass fraction
α_e = nozzle divergence half-angle
γ = ratio of specific heats
δ = velocity boundary-layer thickness at nozzle exit
δ^* = displacement thickness at nozzle exit
δ_t = total enthalpy defect thickness at nozzle exit
η = laser chemical efficiency
θ = momentum defect thickness at nozzle exit
μ = viscosity
ρ = density
ϕ_{ij} = mixture viscosity function
ψ = diluent ratio
ω = viscosity exponent
Ω = total diluent to fluorine ratio

Subscripts and Superscripts

$b\ell$ = edge of boundary layer
c = cold reaction
e = radial core flow at nozzle exit
f = uniform, unmixed parallel flow
g = conditions on transverse plane at nozzle exit
h = hot reaction
i = species i
m = conditions after mixing and before heat addition
mx = conditions in mixing layer
0 = stagnation value
ox = oxidizer
p = primary or oxidizer flow
r = conditions after heat addition
s = secondary or fuel flow
w = wall
$( )^*$ = throat

I. Introduction

IN this study the design and operating conditions are investigated that can lead to choking of the supersonic flow in the optical cavity of an HF or DF laser. Choking was first occasionally observed around 1970 in early laser tests[1] where it was referred to as the PT-56 syndrome. PT-56 is the designation of the transducer that measured the static wall pressure close to the nozzle exit plane. When the amount of oxidizer diluent was decreased below a critical level, the PT-56 pressure would start to increase rapidly. Simultaneously with this increase, the measured laser power rapidly decreased.

Choking can occur in a confined duct with subsonic or supersonic flow due to heat addition or wall friction. When it does occur, changes take place in the inlet conditions, such as a decrease in mass flow rate. In a supersonic flow that is generated by an array of convergent-divergent nozzles, a shock system would develop inside the divergent part of either the fuel and/or oxidizer nozzles. As a consequence of this change in inlet conditions, the calculation that correctly predicts the onset of choking is itself not a valid calculation for the choked flow. A distinction must be made between shock waves caused by choking and shock waves that are normally present in the cavity flow. For example, these later waves are caused by the base region that separates the fuel and oxidizer nozzles,[2] and they occur at all dilution levels. Shock waves are present in the cavity flow even when it is far from choked.

Our interest is restricted to choking caused by the exothermic reactions in the supersonic cavity flow of a cw HF or DF cold-reaction pumped chemical laser. Of particular

Received July 13, 1981; revision received Jan. 25, 1982.

*Professor, Department of Aerospace, Mechanical and Nuclear Engineering. Associate Fellow AIAA.

interest is the effect of the type and amount of diluent, He or N_2, the effect of nozzle geometry, and the effect of diatomic fluorine that exothermically reacts in the cavity via the hot reaction.

This work represents the first systematic investigation of choking for this technology. It is timely because of interest in decreasing the amount of diluent, changing from He to N_2 diluent, and testing with shrouds that confine the cavity flow to a constant area.[3] These trends in the combustor-driven chemical laser technology make desirable a quantitative prediction of how close a given test condition is to choking.

The chosen parameters, and a range of values for them, have been established over the years by laser testing.[3-9] The parametric investigation centers around two nominal cases, one for He diluent, the other for N_2, using typical combustor conditions (pressure, temperature, and composition). These and other conditions then are varied systematically. Although choking is due to heat addition in the cavity, the analysis must start in the oxidizer and fuel plenums because of the influence of parameters such as the stagnation temperatures and the large viscous losses in the small nozzles.

Because of the extensive nature of the calculations and the number of parameters examined, a number of simplifying approximations are utilized. The most important of these are now discussed. The first one is the assumption of a constant cross-sectional area for the cavity, which optimizes a diffuser produced recovered pressure[2] and is the configuration most suitable for scaling test results to nozzle banks of a larger height. Furthermore, this configuration represents a conservative approximation for a choking analysis. A second approximation is the use of one-dimensional flow equations for the core flow in the nozzles and for the mixing and reaction processes in the cavity. Their use in the later situation is discussed in Ref. 2, where a similar approach was first utilized for an examination of the diffuser recovered pressure. Their applicability to a choking analysis is also discussed in Appendix A. Several possible cavity heat addition processes are not included, the most important of these is for H or D atom recombination. An assessment of these processes is contained in Appendix B. Finally, the small base regions that occur between adjacent nozzles is neglected. These regions generate a wake loss[10] that alters the Mach number to an extent depending on the fraction of nozzle bank exit area that is base. This effect can be neglected for those nozzles where the fraction of area that is base is small.

In view of the noted assumptions, a comparison with experimental data would be desirable. Such data, however, are not available. The value of this analysis is thus limited to 1) providing a new, relatively simple technique for analyzing choking; 2) a set of guidelines for estimating the likelihood that various trends may lead to, or alleviate, choking; and 3) a scenario for future testing.

The analysis is similar to those that deal with pressure recovery, e.g., Refs. 2, 8, 11, and 12. Pressure recovery depends on the diffuser inlet Mach number, which also governs choking considerations. Methods for determining the recovered pressure, thus, are generally applicable for evaluating choking.

II. Oxidizer or Primary Flow

The oxidizer, or primary, flow is denoted by a p subscript only when necessary for clarity, while the fuel, or secondary, flow is denoted by an s subscript only when required for clarity. For an HF laser, the thermal source in the combustor plenum frequently is provided by the energetic D_2+F_2 reaction, which dissociates the excess fluorine. Since not all of the F_2 is necessarily dissociated, or some atomic fluorine may recombine on the nozzle wall,[13] the nozzle discharge consists of $F+F_2+DF+$diluent. For simplicity, we neglected the DF constituent since its mole fraction is small compared to that of the diluent.[2] Primary flow composition is then specified in terms of

$$\alpha=\dot{N}_F/(\dot{N}_F+2\dot{N}_{F_2}), \qquad \psi=\frac{\dot{N}_{He_p}+\dot{N}_{N_2}}{0.5\dot{N}_F+\dot{N}_{F_2}} \tag{1}$$

where $\dot{N}_i$ is the molar flow rate of species i. The parameter α is the fluorine atom mass fraction, while ψ_p is the diluent/oxidizer mole ratio. Except for atomic fluorine, the primary flow rates and molecular weight are given by

$$\dot{N}_{F_2}=(1-\alpha)\dot{N}_F/(2\alpha), \qquad \dot{N}_{He_p}=(1-j_1)\psi_p\dot{N}_F/(2\alpha)$$

$$\dot{N}_{N_2}=j_1\psi_p\dot{N}_F/(2\alpha)$$

$$W_p=2[19+2(1+6j_1)\psi_p]/(1+\alpha+\psi_p) \tag{2}$$

For both the primary and secondary flows, we assume a two-dimensional wedge nozzle of unit height with a discharge coefficient of unity. The fluorine-atom flow rate is then provided by the relation

$$\dot{N}_F=\frac{111\alpha}{19+2(1+6j_1)\psi_p}\left[\left(\frac{2}{\gamma+1}\right)^{(\gamma+1)/2(\gamma-1)}\left(\frac{\gamma W}{T_0}\right)^{1/2}p_0y^*\right] \tag{3}$$

where a zero subscript denotes stagnation conditions, and y^* is the throat half width. The ratio of specific heats is given by

$$\gamma=\frac{2\alpha\gamma_1/(\gamma_1-1)+(1-\alpha)\gamma_2/(\gamma_2-1)+[(1-j_1)\gamma_3/(\gamma_3-1)+j_1\gamma_4/(\gamma_4-1)]\psi_p}{2\alpha/(\gamma_1-1)+(1-\alpha)/(\gamma_2-1)+[(1-j_1)/(\gamma_3-1)+j_1/(\gamma_4-1)]\psi_p} \tag{4}$$

where the γ_i are given in Table 1. Specification of p_0, T_0, y^*, j_1, α, and ψ_p fix the primary flow, which is determined before solving for the subsequent nozzle flow.

Nozzle flow is treated in a manner similar to that used by Russell[14,15] for grid nozzles, where a laminar boundary layer develops along the divergent walls of the wedge nozzles. Since the oxidizer and fuel nozzle exit pressures are not necessarily equal, it is possible for the boundary layer of one of the nozzles to separate. For simplicity, we neglect this effect. With Prandtl number equal to unity and a constant density-viscosity product, the displacement thickness at the nozzle exit can be approximated by[15]

$$\frac{\delta^*}{y^*}=\frac{(A_g/A^*)-1}{Re_x^{1/2}\sin\alpha_e}[1.72(T_w/T_e)+0.332(\gamma-1)M_e^2] \tag{5}$$

Table 1 Species properties

Nozzle	i	Species	W_i, g/mole	γ_i	C_i, g/cm-s, $\times 10^{-6}$	ω_i
Primary	1	F	19	1.667	3.8	0.706
	2	F_2	38	1.34	4.3	0.703
	3	He	4	1.667	4.0	0.685
	4	N_2	28	1.4	3.2	0.705
Secondary	5	H_2	2	1.4	2.1	0.660
	6	D_2	4	1.4	3.1	0.648
	7	He	4	1.667	4.0	0.685

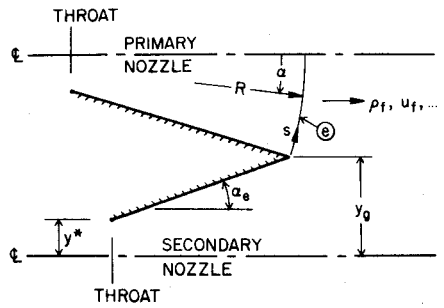

Fig. 1 Schematic showing two-dimensional wedge nozzles and geometrical notation.

where A_g/A^* is the nozzle's geometric area ratio y_g/y^*. As shown in Fig. 1, the e subscript denotes quantities on the circular arc at the nozzle's exit. Thus, M_e is related to the flow area ratio by the isentropic relation

$$\frac{A_g}{A^*}\frac{\alpha_e}{\sin\alpha_e}-\frac{\delta^*}{y^*}=\frac{1}{M_e}\left[\left(\frac{2}{\gamma+1}\right)\left(1+\frac{\gamma-1}{2}M_e^2\right)\right]^{\frac{\gamma+1}{2(\gamma-1)}} \tag{6}$$

where the left side is derived in Appendix C. The Reynolds number in Eq. (5) can be written as

$$Re_x=\left(\frac{A_g}{A^*}-1\right)(Re_0)\frac{M_e}{\sin\alpha_e}\left[1+(\gamma-1)M_e^2/2\right]^{\omega-\frac{\gamma+1}{2(\gamma-1)}} \tag{7}$$

where ω is the viscosity exponent (see Table 1), and Re_0 is a Reynolds number defined by

$$Re_0=a_0\rho_0 y^*/\mu_0 \tag{8}$$

The mixture viscosity is given by a Wilkie-type formula

$$\mu_0=T_0^{\omega}\sum_i\frac{C_iX_i}{X_i+(1/2\sqrt{2})\Sigma x_j\phi_{ij}},\qquad \phi_{ii}=0$$

$$\phi_{ij}=\frac{[1+(C_i/C_j)^{1/2}(W_j/W_i)^{1/4}]^2}{[1+(W_i/W_j)]^{1/2}},\qquad i\neq j \tag{9}$$

In the above, the C_i and molecular weights W_i are given in Table 1, X_i is the mole fraction of species i, and the i and j summations are from 1 to 4 for the primary flow, and 5 to 7 for the secondary flow. These equations are solved on a computer for all desired quantities, such as δ^*, M_e, etc.

The final primary flow calculation turns the radially expanding flow into a parallel, uniform one, where the pertinent equations are derived in Appendix C. This evaluation accounts for the compression necessary for the turn[15] and averages the nozzle viscous losses over the entire primary flow. In addition to the boundary-layer assumption, we also assume θ and δ_t small compared to the displacement thickness δ^*. As shown in Appendix C, the not-too-thick boundary-layer requirement is a mild one, while the second assumption is generally applicable when the nozzle area ratio is 10 or larger.[2,15] Consequently, the Appendix C equations can be written as

$$\dot{m}=\left[\frac{\alpha_e}{\sin\alpha_e}\frac{A_g}{A^*}-\frac{\delta^*}{y^*}\right]\rho_e u_e y^* \tag{10a}$$

$$H_f=H_e \tag{10b}$$

$$J=p_fA_g+\rho_f u_f^2A_g=\left[p_e\frac{A_g}{A^*}+\left(\frac{A_g}{A^*}-\frac{\delta^*}{y^*}\cos\alpha_e\right)\rho_e u_e^2\right]y^* \tag{10c}$$

Equation (10a) is continuity expressed in terms of known quantities; Eq. (10b) expresses the result that the flow in the divergent part of the nozzle is adiabatic. In Eq. (10c) J is the impulse. Equations (10) are not used to determine p_f, ρ_f, etc., since these quantities are not utilized in any subsequent calculation. The quantities of direct use are $\dot{m}$, the adiabatic flow result, and J.

III. Secondary Flow

The secondary flow consists of H_2 or D_2 fuel and He diluent. Secondary N_2 diluent is not considered, since its use is known to rapidly degrade laser power. Furthermore, when N_2 is the primary diluent, no secondary He diluent is used. (Storage of two diluents is impractical. Excess secondary H_2 or D_2 is preferred.)

The secondary flow composition is given in terms of a diluent ratio ψ_s and a fuel/oxidizer ratio R_L

$$\psi_s=\dot{N}_{\mathrm{He}_s}/(\dot{N}_{\mathrm{H}_2}+\dot{N}_{\mathrm{D}_2}),\quad R_L=(\dot{N}_{\mathrm{H}_2}+\dot{N}_{\mathrm{D}_2})/(0.5\dot{N}_{\mathrm{F}}+\dot{N}_{\mathrm{F}_2}) \tag{11}$$

The secondary flow molecular weight, specific heat ratio, and molar flow rates are given by

$$W_s=2(1+j_2+2\psi_s)/(1+\psi_s)$$

$$\gamma=\frac{(1-j_2)\gamma_5/(\gamma_5-1)+j_2\gamma_6/(\gamma_6-1)+\gamma_7\psi_s/(\gamma_7-1)}{(1-j_2)/(\gamma_5-1)+j_2/(\gamma_6-1)+\psi_s/(\gamma_7-1)}$$

$$\dot{N}_{\mathrm{H}_2}=(1-j_2)R_L\dot{N}_{\mathrm{F}}/(2\alpha),\qquad \dot{N}_{\mathrm{D}_2}=j_2R_L\dot{N}_{\mathrm{F}}/(2\alpha)$$

$$\dot{N}_{\mathrm{He}_s}=R_L\psi_s\dot{N}_{\mathrm{F}}/(2\alpha) \tag{12}$$

where α is given by Eq. (1), and $\dot{N}_{\mathrm{F}}$ by Eq. (3). Since $\dot{m}_s=\Sigma W_i\dot{N}_i$, the secondary flow stagnation pressure is obtained by an equation similar to Eq. (3). The subsequent nozzle flow and uniformization calculations exactly parallel those previously described for the primary flow.

IV. Mixed Flow

In the cavity, mixing and reaction occur simultaneously. When the flow has a constant cross-sectional area, however, an exact one-dimensional solution is obtained by sequentially mixing, and then reacting the two streams. This approach has the advantage of being independent of the rate of mixing and the rates of reaction.[2] As a consequence, it is not necessary to know if the mixing is laminar, transitional, or turbulent, and "trip-flow" mixing [3] is encompassed within this approach.

The mixed solution is designated by an m subscript, and is shown to be[2]

$$A_m=\left(\frac{A_g}{A^*}y^*\right)_p+\left(\frac{A_g}{A^*}y^*\right)_s \tag{13a}$$

$$\dot{m}_m=\dot{m}_p+\dot{m}_s \tag{13b}$$

$$\dot{N}_m=\frac{\dot{m}_p}{W_p}+\frac{\dot{m}_s}{W_s} \tag{13c}$$

$$W_m=\frac{\dot{m}_m}{\dot{N}_m} \tag{13d}$$

$$\gamma_m = \frac{[\dot{N}\gamma/(\gamma-1)]_p + [\dot{N}\gamma/(\gamma-1)]_s}{[\dot{N}/(\gamma-1)]_p + [\dot{N}/(\gamma-1)]_s} \tag{13e}$$

$$T_{0m} = \frac{[\gamma\dot{N}T_0/(\gamma-1)]_p + [\gamma\dot{N}T_0/(\gamma-1)]_s}{[\gamma\dot{N}/(\gamma-1)]_m} \tag{13f}$$

$$J_m = J_p + J_s \tag{13g}$$

$$Z_m = 1 - 2R\left[\frac{\gamma+1}{\gamma}\frac{T_0}{W}\left(\frac{\dot{m}}{J}\right)^2\right]_m \tag{13h}$$

$$M_m = \left(\frac{1+Z_m^{1/2}}{1-\gamma_m Z_m^{1/2}}\right)^{1/2} \tag{13i}$$

In the preceding, the equation for the mixture stagnation temperature, T_{0m}, is a consequence of the adiabatic result of the preceding section. In the Z_m equation, R is the universal gas constant. The parameter Z_m is a dimensionless mixing parameter, originally introduced in Ref. 2. For the mixed flow to be supersonic, Z_m must fall in the range $0 \le Z_m \le \gamma_m^{-2}$.

V. Reacted Flow

We assume the cold and hot reactions,

$$F + H_2 \rightarrow HF + H, \qquad F_2 + H \rightarrow HF + F$$

or their deuterium analogs, go to completion, and the presence of sufficient H_2 such that all the F and F_2 are converted to HF. This last condition simplifies the heat addition calculation. To obtain maximum heat addition, all collisional deactivation processes are assumed to go to completion. For simplicity, the ratio of specific heats is assumed to be constant with a value equal to γ_m. This approximation is justified when changes in composition and temperature are not extreme, as is the case when a large amount of diluent is present. The molecular weight and molar flow rate are unchanged, since only binary reactions are occurring.

It is convenient to introduce Ω, the ratio of the total amount of diluent, after complete reaction, to the initial fluorine, considered as F_2. As part of the diluent we include excess H_2 (or D_2) and the HF and H species (or DF and D) produced by the given reactions. Hence, Ω is given by

$$\Omega = \frac{\dot{N}_{He_p} + \dot{N}_{N_2} + \dot{N}_{He_s} + \dot{N}_{H_2} + \dot{N}_{D_2} + \dot{N}_F + \dot{N}_{F_2}}{0.5\dot{N}_F + \dot{N}_{F_2}}$$

$$= \psi_p + (1+\psi_s)R_L + 1 + \alpha \tag{14}$$

Since the numerator of the middle expression equals the total molar flow rate $\dot{N}_m$, and with Eq. (2), Ω can be written as $2\alpha\dot{N}_m/\dot{N}_F$.

Although our principal interest is in the cold reaction pumped laser, some hot reaction also occurs when $\alpha < 1$. The heat addition, in kJ/mole, for the two reactions is

$$-\Delta H_c = 4.184(31.6 - j_2) \qquad -\Delta H_h = 4.184(98 + 1.4j_2)$$

Relative to the pure cold reaction case, the fractional increase in cavity heat addition due to the hot reaction is

$$\frac{1+\alpha}{2} + \frac{1-\alpha}{2}\frac{\Delta H_h}{\Delta H_c} \tag{15}$$

When $\alpha = 0.7$ there is approximately 32% more heat addition than when $\alpha = 1$.

The extracted laser power P is determined in terms of an efficiency η, which, by convention, considers all the fluorine to be dissociated. The efficiency is thus given by

$$\eta = P/\{(\dot{N}_F + 2\dot{N}_{F_2})|\Delta H_c|\} \tag{16}$$

which can be rewritten as

$$\frac{P}{\dot{m}} = \frac{2\eta|\Delta H_c|}{W_m\Omega} \tag{17}$$

A dimensionless heat addition parameter Z_r can be defined as[2]

$$Z_r = 1 + \frac{\gamma_m - 1}{\gamma_m}\frac{(1-\alpha-2\eta)|\Delta H_c| + (1-\alpha)|\Delta H_h|}{RT_{0m}\Omega} \tag{18}$$

where Z_r is the ratio of the final stagnation temperature to that before heat addition. After some algebraic manipulation, the final supersonic Mach number M_r can be shown to equal

$$M_r^2 = \frac{1 + [1 - Z_r(1-Z_m)]^{1/2}}{1 - \gamma_m[1 - Z_r(1-Z_m)]^{1/2}} \tag{19}$$

Other quantities, such as pressure or temperature, are readily determined, but are not needed here.

Inspection of Eq. (19) shows that choking, where $M_r = 1$, occurs when

$$Z_r(1 - Z_m) = 1 \tag{20}$$

Either M_r or the point (Z_m, Z_r) may be used as a measure of how close the flow is to choking. It is evident from Eq. (19) that whether or not the flow chokes depends solely on three dimensionless parameters: γ_m, Z_m, and Z_r. The latter two parameters demonstrate the importance of the average stagnation temperature (before heat addition) T_{0m}, the impulse per unit mass $J_m/\dot{m}_m$, W_m, Ω, and the overall heat addition.

VI. Results

The parameter values for the two nominal cases, Table 2, are typical of combustor driven lasers. Aside from diluent, only the secondary nozzle and associated flow conditions

Table 2 Parameter values for nominal cases

Parameter	He case	N_2 case
Common		
Laser efficiency η	0.1	0.1
Wall temperature T_w, K	3×10^2	3×10^2
Primary nozzle		
Area ratio A_g/A^*	20	20
Throat size y^*, cm	5×10^{-3}	5×10^{-3}
Divergence angle α_e, deg	15	15
Stagnation pressure p_0, atm	10	10
Stagnation temperature T_0, K	1.5×10^3	1.5×10^3
Diluent ratio ψ	20	20
F-atom ratio α	1	1
Viscosity exponent ω	0.7	0.7
Secondary nozzle		
Area ratio A_g/A^*	20	10
Throat size y^*, cm	5×10^{-3}	5×10^{-3}
Divergence angle α_e, deg	15	15
Stagnation temperature T_0, K	3×10^2	3×10^2
Fuel	H_2	H_2
Diluent ratio ψ	5	0
Fuel/oxidizer ratio R_L	2	12
Viscosity exponent ω	0.68	0.68

Table 3 Nozzle results for nominal cases

Parameter	He case	N_2 case
Primary nozzle		
Reynolds number Re_0	6.3×10^2	1.64×10^3
Displacement thickness δ^*/y_g	0.283	0.109
Core Mach number M_e	5.82	4.68
Exit pressure p_e, atm	1.89×10^{-2}	2.90×10^{-2}
Exit impulse J, g-cm/s^2	8.06×10^4	8.45×10^4
Mass flow rate $\dot{m}$, g/s	0.241	0.514
Secondary nozzle		
Reynolds number, Re_0	8.86×10^2	2.38×10^2
Stagnation pressure p_0, atm	2.04	0.664
Displacement thickness δ^*/y_g	0.260	0.298
Core Mach number M_e	5.46	3.55
Exit pressure p_e, atm	4.48×10^{-3}	8.07×10^{-3}
Exit impulse J, g-cm/s^2	1.67×10^4	5.56×10^3
Mass flow rate $\dot{m}$, g/s	8.99×10^{-2}	2.06×10^{-2}

differ. A smaller value for $(A_g/A^*)_s$ is used with N_2 in order to reduce the nozzle exit pressure ratio p_{ep}/p_{es}. Too large a value for this ratio implies boundary-layer separation inside the secondary nozzle. Partly for the same reason, R_L has been increased to 12 to compensate for the removal of He from the secondary flow. This change fixes the diluent/fluorine ratio Ω at 34 for both cases.

Results from the primary and secondary nozzle solutions are shown in Table 3. The small Re_0 values stem from the small throat size. By ordinary boundary-layer theory standards, the flow in the nozzles is highly viscous, with δ^*/y_g ranging from 0.1 to 0.3. For both cases the ratio p_{ep}/p_{es} is about 4. The total impulse J_p+J_s is also about the same for both cases. The N_2 mass flow rate, however, exceeds that for the He case by a factor of 1.6. Consequently, Z_m for N_2 exceeds that for He. One final point of interest is the low secondary stagnation pressure p_{0s} as compared to p_{0p}. In turn, this results in a small value for J_s relative to J_p.

Results for the He diluent study are presented in Tables 4a-d. In Table 4a results are given for the nominal case and for a variation in laser efficiency η and wall temperature T_w. Z_m, Z_r, and M_r are tabulated, along with the mixed flow Mach number M_m. In contrast to M_r, M_m is rather artificial and its value is shown for reference purposes only. In view of the large core Mach numbers shown for He diluent in Table 3, the decrease to M_m and M_r is substantial. It is worth noting that the change in Mach number from $M_m=4.30$ to $M_r=1.64$ is due solely to heat addition produced by the cold reaction.

As expected, the more efficient lasing case (Table 4a) has the highest Mach number, while a change in T_w has little influence, since only Eq. (5) is affected by this change.

Table 4b presents results of seven different variations grouped under the heading of primary nozzle. The first variation, for p_{0p}, shows little change until p_{0p} is small; then Z_m (because of the nonlinear behavior of J_p) and M_r rapidly increase. (At low p_{0p}, when M_m is large, the second law of thermodynamics can be shown to be violated by the mixing calculation.) The second variation, for T_{0p}, shows the rather strong effect this parameter has on Z_r and M_r. Choking is certainly more likely with large combustor heat transfer losses, and, hence a small T_{0p}. A decrease in ψ_p to 10 is sufficient to choke the flow, while an increase to 30 increases M_r to 2.

A decrease in the F-atom ratio α from 1 to 0.7 decreases M_r. This variation is shown as curve A in Fig. 2, a Z_m, Z_r plot. Also shown are the boundaries delineating the region where M_m and M_r are supersonic. Since a change in α primarily involves a change in cavity heat addition, curve A is vertical. Other changes, such as in nozzle geometry, primarily alter the mixing and thereby generate a horizontal curve.

The final three variations in Table 4b alter the primary nozzle geometry. Despite the extent of the variations, there is only a minimal effect on M_r. The reason for this is the

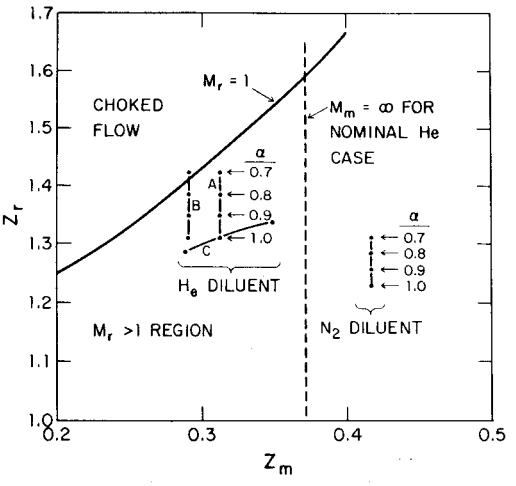

Fig. 2 Z_m, Z_r plot. Curves A and B are for $(A_g/A^*)_p=(A_g/A^*)_s=20$ and $(A_g/A^*)_p=(A_g/A^*)_s=10$, respectively. Curve C is for a change in ψ_s (Table 4c). The dashed vertical line shows where $M_m=\infty$ for He diluent, the equivalent N_2 line is at $Z_m=0.503$.

relatively weak dependence of $J/\dot{m}$ on Mach number

$$\frac{J}{\dot{m}}=\left(\frac{\gamma+1}{2}\right)^{1/2}\frac{a^*}{\gamma}\,\frac{1+\gamma M^2}{M[1+(\gamma-1)M^2/2]^{1/2}} \tag{21}$$

where a^* is the speed of sound at Mach one.

Table 4c presents results of six variations grouped under the heading of secondary nozzle. As expected, a shift from H_2 to D_2 fuel causes a negligible change. The next variation provides a surprising result; the case with no added secondary diluent ($\psi_s=0$ and $\Omega=24$) has the largest value for M_r. Thus, the effect of an increased stagnation temperature T_{0m} offsets the effect of reduced dilution. This variation produces curve C in Fig. 2, with the nondilution case as the rightmost point. (By contrast, a variation of ψ_p produces a nearly vertical curve, since T_{0m} is not changing as rapidly.) The effect of a change in ψ_s is most pronounced when ψ_s is small, as can be seen by comparing M_r for $\psi_s=0$ and $\psi_s=10$ with the nominal case, or by observing the location of their Z_m, Z_r points in Fig. 2. In accord with these remarks, the R_L variation, with $R_L=2$ as nominal, has little effect on M_r. As is the case for the primary nozzle, we note little change resulting from changes in the secondary nozzle geometry.

Table 4d shows results when more than one parameter is altered from the He nominal values. The first case doubles the wall temperature and secondary flow stagnation temperature, with the later dominant in increasing M_r. The next two cases replace the secondary He with H_2, while keeping Ω fixed at 34. The small decreases that occur in T_{0m} and $\dot{m}_m$ are sufficient to slightly increase M_r. The following two cases again keep Ω fixed, but shift He from the hot oxidizer flow to the 300 K fuel flow. A shift of half the oxidizer He used in the nominal case causes the flow to choke. This shift decreases T_{0m} from 1059 K (nominal case) to 714 K, thereby causing a large increase in Z_r. The next case tests Reynolds number scaling by adjusting p_{0p}, y_p^*, and y_s^*, with Re_{0p} and Re_{0s} fixed. The change in y_s^* is necessary, since the two flows are coupled through the fixed parameter R_L. This change does not alter Z_m or Z_r, thereby demonstrating this scaling as far as choking is concerned. The final variation considers $\alpha<1$ with smaller nozzle area ratios. Individually neither change resulted in choking. When coupled, however, choking occurs at $\alpha=0.7$. This variation is shown in Fig. 2 as curve B, where we observe that the geometry change has shifted curve A to the left.

The N_2 diluent variation is summarized in Table 5. For the nominal case M_r is 2.47, which is higher than for the nominal He case. This increase is primarily due to the decrease in $J/\dot{m}$ alluded to earlier. It should be noted that this result runs

Table 4a Mach number results for single parameter variation about He nominal case—common factors

Parameter	Parameter value	Z_m	M_m	Z_r	M_r
Nominal case	—	0.3111	4.30	1.311	1.64
Laser efficiency η	0	0.3111	4.30	1.345	1.51
	0.2	0.3111	4.30	1.276	1.77
Wall temperature T_w	6×10^2	0.3123	4.35	1.311	1.65
	9×10^2	0.3137	4.40	1.311	1.66

Table 4b Mach number results for single parameter variation about He nominal case—primary nozzle

Parameter	Parameter value	Z_m	M_m	Z_r	M_r
Pressure p_0	1	0.3535	8.17	1.311	1.97
	5	0.3181	4.60	1.311	1.69
	15	0.3082	4.19	1.311	1.62
Temperature T_0	1.2	0.3192	4.65	1.379	1.45
	1.8×10^3	0.3040	4.05	1.264	1.77
Diluent ratio ψ_p	10	0.3161	4.35	1.524	ch
	30	0.3123	4.43	1.221	2.03
F-atom ratio α	0.9	0.3117	4.30	1.348	1.51
	0.8	0.3123	4.30	1.385	1.38
	0.7	0.3123	4.29	1.422	1.24
Area ratio A_g/A^*	10	0.2933	3.73	1.311	1.51
	30	0.3190	4.64	1.311	1.70
Throat width y^*	2.5×10^{-3}	0.3181	4.60	1.311	1.69
	7.5×10^{-3}	0.3082	4.19	1.311	1.62
Divergence angle α_e	7.5	0.3161	4.51	1.311	1.67
	22.5	0.3027	4.00	1.311	1.58

Table 4c Mach number results for single parameter variation about He nominal case—secondary nozzle

Parameter	Parameter value	Z_m	M_m	Z_r	M_r
Cavity fuel	D_2	0.3046	4.07	1.301	1.63
Diluent ratio ψ_s	0	0.3485	6.59	1.338	1.81
	10	0.2884	3.65	1.287	1.57
Fuel/oxidizer ratio R_L	4	0.2994	3.79	1.282	1.66
	6	0.2941	3.60	1.257	1.71
Area ratio A_g/A^*	10	0.3072	4.15	1.311	1.61
	30	0.3128	4.37	1.311	1.65
Throat width y^*	2.5×10^{-3}	0.3111	4.30	1.311	1.64
	7.5×10^{-3}	0.3111	4.30	1.311	1.64
Divergence angle α_e	7.5	0.3123	4.35	1.311	1.65
	22.5	0.3092	4.23	1.311	1.62

Table 4d Mach number results for multiple parameter variations about He nominal case

Parameter values	Rationale	Z_m	M_m	Z_r	M_r
$T_w = T_{0s} = 600$	Heated secondary	0.3382	5.91	1.282	1.96
$R_L = 4, \psi_s = 2$	Vary secondary	0.3295	4.71	1.309	1.76
$R_L = 6, \psi_s = 1$	flow with $\Omega = 34$	0.3463	5.13	1.307	1.88
$\psi_p = 10, \psi_s = 10$	Vary diluent	0.2970	3.83	1.461	ch
$\psi_p = 15, \psi_s = 7.5$	ratios with $\Omega = 34$	0.2994	3.90	1.371	1.33
$p_{0p} = 1, y_p^* = y_s^* = 0.05$	Constant Re_0	0.3111	4.30	1.311	1.64
$(A_g/A^*)_p = (A_g/A^*)_s = 10$	Reduced area				
$\alpha = 1$	ratios with	0.2893	3.63	1.311	1.49
$\alpha = 0.9$	varying F-atom	0.2898	3.62	1.348	1.35
$\alpha = 0.8$	ratio	0.2904	3.62	1.385	1.20
$\alpha = 0.7$		0.2909	3.62	1.422	ch

counter to intuition in view of the smaller γ_m (1.41 compared to 1.64 for the He case) and the smaller nozzle core Mach numbers for both the primary and secondary flows (see Table 3).

Trends shown in Table 5 are the same as in Tables 4, except for the $T_w = T_{0s} = 600$ K case. In contrast to the comparable case in Table 4d, the increase in T_{0m} is not offset by an increase in $J/\dot{m}$, thereby resulting in a decrease in Z_m from the nominal value. Of particular interest is the α variation, which is shown in Fig. 2. It is clear from this figure and Table 5 that N_2 diluent flow should be able to tolerate a larger cavity heat addition than a comparable He flow.

Table 5 Mach number results for parameter variation about N_2 nominal case

Parameter	Parameter value	Z_m	M_m	Z_r	M_r
Nominal case	—	0.4163	4.26	1.229	2.47
Laser efficiency η	0	0.4163	4.26	1.254	2.37
	0.2	0.4163	4.26	1.203	2.59
Primary pressure p_{0p}	1	0.4317	4.74	1.223	2.62
	5	0.4186	4.33	1.223	2.49
Primary temperature T_{0p}	1.2×10^3	0.4098	4.10	1.279	2.22
	1.8×10^3	0.4203	4.38	1.194	2.67
Primary diluent ratio ψ_p	10	0.4094	4.15	1.394	1.87
	30	0.4197	4.32	1.161	2.83
F-atom ratio α	0.9	0.4166	4.25	1.256	2.36
	0.8	0.4169	4.24	1.283	2.26
	0.7	0.4172	4.23	1.310	2.17
Primary area ratio A_g/A^*	10	0.3880	3.65	1.229	2.24
Cavity fuel	D_2	0.4231	4.46	1.222	2.57
Fuel/oxidizer ratio R_L	7	0.4193	4.37	1.239	2.46
	2	0.4221	4.50	1.250	2.45
Heated wall and secondary $T_w = T_{0s}$	6×10^2	0.3902	3.69	1.208	2.34

VII. Summary

An analytical procedure is provided for determining if thermal choking is close to occurring in a cw supersonic chemical laser. The most important results of a parametric investigation are as follows.

1) Relative to He diluent, choking is less likely with N_2 diluent.

2) Reynolds number scaling applies provided both the fuel and oxidizer nozzles are scaled.

3) The oxidizer stagnation temperature T_{0p} and diluent ratio ψ_p have a strong influence on the possibility of choking. Shifting oxidizer diluent to the fuel flow tends to cause choking.

4) The fluorine atom mass fraction α has only a moderate influence on choking for $\alpha \geq 0.7$.

5) The fuel diluent ratio ψ_s and fuel/oxidizer ratio R_L have little influence on choking. An interesting result is the weak choking dependence on the geometry for either the oxidizer or fuel nozzles.

Appendix A: Choking in a Nonuniform Flow

It is not evident that choking based on a one-dimensional, uniform-state approach is equivalent to choking in a real laser flow where at any cavity cross section flow conditions are nonuniform. As shown by the results of Navier-Stokes calculations for a wedge-shaped nozzle array with a finite area base region,[16] there are transverse pressure gradients early in the cavity flow which decay rapidly as the flow progresses downstream. A "leaky-tube" mixing model[17] thus provides an appropriate, but simple, vehicle for considering choking in a nonuniform flow. In this model adjacent streamtubes have different temperatures, Mach numbers, and composition, but are at the same local static pressure. Three streamtubes are involved; one each for the oxidizer and fuel and a middle one where the entrained constituents react. The choking condition for this model is given in Ref. 17 as

$$\left(A\frac{M^2-1}{\gamma M^2}\right)_{ox}+\left(A\frac{M^2-1}{\gamma M^2}\right)_{fuel}+A\left(\frac{M^2-1}{\gamma M^2}\right)_{mx}=0 \quad \text{(A1)}$$

where A_{ox} and M_{ox} are the local cross-sectional area and average Mach number of the oxidizer flow, respectively. Note that when the flow is fully mixed, $A_{ox}=A_{fuel}=0$, the usual condition, $M_{mx}=1$, is obtained for choking.

Whenever $M>1$, the factor $(M^2-1)/M^2$ is between zero and unity. Hence, with M_{ox} and M_{fuel} supersonic and $A_{ox}+A_{fuel}>0$, choking can occur only if M_{mx} has decreased from its initial supersonic value to one that is subsonic. In this formulation it is possible for M_{mx} to go smoothly through unity with increasing axial distance without the flow choking.

For purposes of discussion, assume isentropic flow for the fuel and oxidizer streams with supersonic initial values. The heat addition, which occurs solely in the mixing layer, is generally adequate to cause a substantial adverse pressure gradient. Both the heat addition and this pressure gradient result in a decreasing value with distance for M_{mx}, which initially is also supersonic. Both M_{ox} and M_{fuel} decrease because of the pressure gradient. If the adverse pressure gradient and heat release are large enough, a location may be reached where M_{mx} is sufficiently subsonic for the flow to choke. The oxidizer and fuel supersonic Mach numbers are then inadequate to counter in Eq. (A1) the negative mixing term.

Appendix B: Additional Cavity Thermal Sources

Two cavity heat addition processes not included in the formulation are H-atom recombination and, when N_2 is the oxidizer diluent, collisional deactivation of vibrationally excited N_2. The vibrational energy of the hot N_2 might well freeze when flowing through the small oxidizer nozzles. If rapid freezing occurs, then the N_2 vibrational energy is 3.284 kJ/mole when $T_{0p}=1500$ K.[18] For the nominal N_2 case, the corresponding cavity heat addition, relative to that from the cold reaction, is given by

$$\frac{N_2 \text{ vib. energy}}{\text{cold reaction}}=\frac{\Delta H_{N_2}\dot{N}_{N_2}}{\Delta H_c\dot{N}_F}=\frac{\Delta H_{N_2}\psi_p}{\Delta H_c 2}=0.25$$

Thus, N_2 vibrational excitation can increase the cavity heat addition, when $\alpha=1$, by about 25%. This is of the same magnitude as that caused by undissociated F_2 and, hence, this effect leads to comparable Mach number changes.

The cold reaction produces a copious amount of H or D atoms, whose three-body recombination is highly exothermic. For example, when $\alpha=1$, the recombination heat addition, relative to the cold reaction, is given by

$$\frac{\text{H-atom recomb.}}{\text{cold reaction}}=\frac{\Delta H_h\dot{N}_H}{\Delta H_c\dot{N}_F}=\frac{52}{31.6}=1.65$$

This heat addition would choke most laser flows if it fully occurred. Since this choking has not been experimentally observed, a significant amount of recombination does not appear to occur. Further verification of this conclusion can be obtained by estimating for the mixing layer an H-atom

recombination length using rate coefficients from Ref. 19. With typical He or N_2 cavity conditions ($\Omega=25$, $T=400$ K, $u=10^5$ cm/s, $p=20$ Torr), one can then show that recombination in the mixing layer is two orders of magnitude too slow to be relevant. This estimate suggests that H or D atoms recombine downstream of the cavity.

Appendix C: Derivation of Equations for Uniform Parallel Flow

A succinct derivation is provided for conversion of the radial flow at station e, which consists of boundary layer plus core flow, into a parallel uniform flow, denoted by an f subscript. Figure 1 should be consulted for the definition of all geometrical quantities. The radial flow is generated by a two-dimensional wedge nozzle with no base area between adjacent nozzles and the streams remain unmixed between stations e and f.

It is important to note that core conditions must be evaluated on the circular arc e. Thus, the area ratio for determining M_e is given by

$$\frac{A_e}{A^*}=\frac{R\alpha_e-\delta^*}{y^*}=\frac{(y_g/\sin\alpha_e)\alpha_e-\delta^*}{y^*}=\left(\frac{\alpha_e}{\sin\alpha_e}\right)\frac{y_g}{y^*}-\frac{\delta^*}{y^*} \tag{C1}$$

since $y_g=R\sin\alpha_e$.

The usual boundary-layer thicknesses are introduced at station e

$$\delta^*=\int_0^\delta\left(1-\frac{\rho u}{\rho_e u_e}\right)ds, \qquad \delta_t=\int_0^\delta\frac{\rho u}{\rho_e u_e}\left(\frac{H}{H_e}-1\right)ds$$

$$\theta=\int_0^\delta\frac{\rho u}{\rho_e u_e}\left(1-\frac{u}{u_e}\right)ds \tag{C2}$$

These relations are used in the following form.

$$R\int_{\alpha_e-\alpha_{b\ell}}^{\alpha_e}\rho u\,d\alpha=(\delta-\delta^*)\rho_e u_e$$

$$R\int_{\alpha_e-\alpha_{b\ell}}^{\alpha_e}\rho uH\,d\alpha=(\delta-\delta^*+\delta_t)\rho_e u_e H_e$$

$$R\int_{\alpha_e-\alpha_{b\ell}}^{\alpha_e}\rho u^2\,d\alpha=(\delta-\delta^*-\theta)\rho_e u_e^2 \tag{C3}$$

where $ds=Rd\alpha$ and $\delta=R\alpha_{b\ell}$; i.e., $\alpha_{b\ell}$ is the angle spanned by the boundary layer at station e.

Conservation of mass flow rate requires

$$\rho_f u_f y_g=\int_0^{R\alpha_e}\rho u\,ds=R\int_0^{\alpha_e-\alpha_{b\ell}}\rho_e u_e\,d\alpha+R\int_{\alpha_e-\alpha_{b\ell}}^{\alpha_e}\rho u\,d\alpha$$

$$=R\rho_e u_e(\alpha_e-\alpha_{b\ell})+(\delta-\delta^*)\rho_e u_e \tag{C4a}$$

Since $R=(y_g/\sin\alpha_e)$ and $R\alpha_{b\ell}=\delta$, Eq. (C4a) becomes

$$\left(\frac{\alpha_e}{\sin\alpha_e}-\frac{\delta^*}{y_g}\right)\rho_e u_e=\rho_f u_f \tag{C4b}$$

which is equivalent to $(\rho uA)_e=\rho_f y_f A_g$.

Conservation of energy is given by

$$\rho_f u_f y_g H_f=\int_0^{R\alpha_e}\rho uH\,ds=R\int_0^{\alpha_e-\alpha_{b\ell}}\rho_e u_e H_e\,d\alpha$$

$$+R\int_{\alpha_e-\alpha_{b\ell}}^{\alpha_e}\rho uH\,d\alpha \tag{C5a}$$

This relation can be rewritten as

$$\left(\frac{\alpha_e}{\sin\alpha_e}-\frac{\delta^*-\delta_t}{y_g}\right)\rho_e u_e H_e=\rho_f u_f H_f \tag{C5b}$$

When $\delta_t\ll\delta^*$, this reduces to $H_e=H_f$.

The final conservation equation is for longitudinal momentum

$$(p_f+\rho_f u_f^2)y_g=\int_0^{R\alpha_e}(p_e+\rho u^2)\cos\alpha\,ds=p_e R\int_0^{\alpha_e}\cos\alpha\,d\alpha$$

$$+\rho_e u_e^2 R\int_0^{\alpha_e-\alpha_{b\ell}}\cos\alpha\,d\alpha+R\int_{\alpha_e-\alpha_{b\ell}}^{\alpha_e}\rho u^2\cos\alpha\,d\alpha \tag{C6a}$$

Two approximations are now utilized. In the rightmost integral $\cos\alpha$ is approximated by an average value of $\cos(\alpha_e-1/2\alpha_{b\ell})$. A not-too-thick boundary layer is also assumed, $(\delta/y_g)<1$, so that

$$\sin(\alpha_e-\alpha_{b\ell})\cong\sin\alpha_e\left[1-\frac{1}{2}\left(\frac{\delta}{y_g}\right)^2\sin^2\alpha_e\right]-\frac{\delta}{y_g}\sin\alpha_e\cos\alpha_e$$

$$\cos(\alpha_e-1/2\alpha_{b\ell})\cong\cos\alpha_e+\frac{1}{2}\frac{\delta}{y_g}\sin^2\alpha_e$$

After some manipulation, we obtain

$$p_e+\left[1-\cos\alpha_e\left(\frac{\delta^*+\theta}{y_g}\right)\left(1+\frac{1}{2}\frac{\delta}{y_g}\frac{\sin^2\alpha_e}{\cos\alpha_e}\right)\right]\rho_e u_e^2=p_f+\rho_f u_f^2 \tag{C6b}$$

The highest-order correction term, which is proportional to δ/y_g, can be neglected. For example, if $(\delta/y_g)=0.5$ (this is not a very thin boundary layer), then

α_e	0	15	30
$\frac{1}{2}\frac{\delta}{y_g}\frac{\sin^2\alpha_e}{\cos\alpha_e}$	0	0.017	0.072

and the error is small even when α_e is 30 deg. It is worth noting that only the momentum equation utilizes the not-too-thick boundary-layer assumption.

Acknowledgments

The author gratefully acknowledges several discussions with Professor D. A. Russell concerning the nozzle boundary layer and uniformization calculation.

References

[1] *Project MESA Data Summary - 1970*, Aerospace Rept. TR-0172 (2779)-3, Nov. 1971.

[2] Grohs, G. and Emanuel, G., "Gas Dynamics of Supersonic Mixing Lasers," *Handbook of Chemical Lasers*, John Wiley and Sons, New York, 1976, pp. 263-388.

[3] Wilson, L. E. and Hook, D. L., "Deuterium Fluoride cw Chemical Lasers," AIAA Paper 76-344, July 1976.

[4]Mirels, H. and Spencer, D. J., "Power and Efficiency of a Continuous HF Chemical Laser," *IEEE Journal of Quantum Electronics,* Vol. QE-7, Nov. 1971, pp. 501-507.

[5]Spencer, D. J., Mirels, H., and Durran, D. A., "Performance of CW HF Chemical Lasers with N_2 or He Diluent," *Journal of Applied Physics,* Vol. 43, March 1972, pp. 1151-1157.

[6]Klopotek, R. D., Nagai, C. K., and Giedt, R. R., "A Comparison of Arc Versus Combustor Operation With an HF/DF Chemical Laser," *Proceedings of the Tenth JANNAF Combustion Meeting,* Pub. 243, Chemical Properties Information Agency, 1973.

[7]Spencer, D. J. and Varwig, R. L., "Experimental CW Chemical Laser Studies," *AIAA Journal,* Vol. 11, July 1973, pp. 1000-1005.

[8]Emanuel, G., "Chemical Laser Fluid Dynamics," TRW Rept. RH-CR-76-5, Feb. 1975.

[9]Hook, D. L., Hobbs, C. W., Ackerman, R. A., Jarvis, S. L., and Hosack, G. A., "HF/DF Chemical Laser Technology Studies," TRW Rept. AFWL-TR-74-150, June 1974.

[10]Grohs, G. L., "Chemical Laser Cavity Mixing and Turbulence," AIAA Paper 76-56, Jan. 1976.

[11]Warren, W. R. Jr., "Reacting Flow and Pressure Recovery Processes in HF/DF Chemical Lasers," *Acta Astronautica,* Vol. 1, May/June 1974, pp. 813-834.

[12]Durran, D. A. and Liu, S. W., "Pressure Recovery in a Constant-Area Diffuser for Chemical Lasers with Nozzle Base Relief," Aerospace Rept. TR-0075(5533)-3, June 1975.

[13]Ferrell, J. E., Kendall, R. M., and Tong, H., "Recombination Effects in Chemical Laser Nozzles," AIAA Paper 73-643, 1973.

[14]Russell, D. A., Neice, S. E., and Rose, P. H., "Screen Nozzles for Gasdynamic Lasers," *AIAA Journal,* Vol. 13, May 1975, pp. 593-599.

[15]Russell, D. A., "Fluid Mechanics of High Power Grid Nozzle Lasers," AIAA Paper 74-223, Jan. 1974.

[16]Ramshaw, J. D., Mjolsness, R. C., and Farmer, O. A., "Numerical Method for Two-Dimensional Steady-State Chemical Laser Calculation," *Journal of Quantitative Spectroscopy and Radiative Transfer,* Vol. 17, Jan. 1977, pp. 149-164.

[17]Emanuel, G., "Numerical Modeling of Chemical Lasers," *Handbook of Chemical Lasers,* John Wiley and Sons, New York, 1976, pp. 469-549.

[18]Vincenti, W. G. and Kruger, C. H. Jr., *Introduction to Physical Gas Dynamics,* John Wiley and Sons, New York, 1965, p. 206.

[19]Cohen, N. and Bott, J. F., "A Review of Rate Coefficients in the H_2-F_2 Chemical Laser System," Aerospace Rept. TR-0076(6603)-2, April 1976.